Oceanologia, corrected, in press
Polish Academy of Sciences
Institute of Oceanology

https://doi.org/10.5697/PWUX9926

Semidiurnal and diurnal barotropic currents in the inner shelf and surf zone of the west coast of India: Measurements and modeling

Yadhunath E. M. [1,*], Jaya Kumar Seelam [2,3], Subeesh M. P. [1], Jai Singh [2], Luis Ryan [2]

Abstract
We study the dynamics of barotropic currents at semidiurnal and diurnal frequency bands in the inner shelf and surf zone off the west coast of India using moored velocity observations. In both the Inner shelf and the Surf zone, the observed current exhibits significant semidiurnal and diurnal energy. The hourly climatology of residual currents exhibits a strong diurnal variability in the barotropic currents in the both regions. A 2D hydrodynamic model, Delft3d, was implemented, and sensitivity experiments were performed to understand the role of wind and wave in the tidal and diurnal variability of barotropic currents in the region. Surf zone barotropic currents in diurnal band are strongly modulated by the winds. However, wind has minimal influence on the barotropic current in the inner shelf. Sensitivity experiments with and without waves show that, apart from wind, wave parameters have significant influence on the diurnal variability of surf zone currents. Analysis further confirms that diurnal currents in the surf zone are primarily wind-driven, while inner shelf currents are mostly tide-dominated. Overall, this study underscores the necessity of incorporating wind, wave, and tidal forcing to realistically simulate nearshore currents in the inner shelf and surf zone along the west coast of India.

Keywords
Barotropic tide; Inner shelf; Wave; Surf zone; Delft3d; ADCP

[1] *Naval Physical and Oceanographic Laboratory, Kochi, India*
[2] *CSIR – National Institute of Oceanography, Goa, India*
[3] *Academy of Scientific & Innovative Research, CSIR–NIO, Goa, India*
***Correspondence**: yadhunath90@gmail.com (Yadhunath, E. M.)

Received: 1 December 2024; **revised:** 10 January 2026; **accepted**: 23 February 2026

1. Introduction

The inner shelf serves as a transitional zone between the surf zone and the mid-shelf (Lentz, 1994). The surf zone extends from the shoreline to the outermost point of wave breaking within the inner shelf and represents the most dynamic part of the nearshore environment (Holman, 1986; Hamm, 1992). Both the inner shelf and surf zone are characterized by complex physical processes, including rip currents, wind-driven currents, and tides that significantly influence the transport and distribution of littorals (Basco, 1983). Tides generally propagate from the inner shelf into the surf zone, whereas wind-induced currents primarily affect the surface layer in the surf zone (Matsunaga et al., 1996; Ren et al., 2015; Paniagua-Arroyave et al., 2019; Sous et al., 2021). Additionally, the nearshore bathymetry modulates wave breaking and current propagation, creating a gradient in current magnitude and direction between these regions (Inman and Quinn, 1951; Longuet-Higgins, 1970b; Wright and Short, 1984; Port et al., 2011). Circulations in the surf zone, which include longshore and cross-shore currents, wave breaking, and associated sediment transport, is particularly important for understanding coastal morphology and its evolution (Basco, 1983; Pitman et al., 2016). The studies show the complex nature of coastal zones and emphasize the importance of integrated approaches for their effective understanding and management (Sharples, 1997; Galparsoro et al., 2010; Delpey et al., 2021; Moulton et al., 2021).

Tidal currents play a particularly important role in shallow coastal waters (Pugh, 1987; Dyer, 1997; Stow, 2017). In these regions, tidal energy dissipation increases drastically, as tidal dissipation is proportional to the cube of the current velocity (Müller, 2012; Alford et al., 2019). Understanding the dynamics and variability of tidal currents is crucial for several reasons. They drive sediment transport,

shaping patterns of coastal erosion and deposition, which in turn influence shoreline stability and marine habitats, transport and accumulation of floating micro plastics (Andutta et al., 2019; Pradhan et al., 2020; Sterl et al., 2020). Tidal currents also affect maritime navigation, impacting the safety and operational efficiency of ports and harbors (Truong et al., 2021). In an open ocean modeling study Halsne et al. (2024) pointed out that wave current interactions are more extreme when the wind sea opposes the tidal current. Moreover, detailed knowledge of these currents is essential for environmental management, particularly in evaluating the effects of anthropogenic activities and natural phenomena such as monsoons (Jiao et al., 2015).

The coastal region of Goa, located along the western coast of India, is known for its rich marine biodiversity and economically vital sectors such as tourism, fishing, and shipping (Alvares, 1993). The inner shelf of Goa is a dynamically complex region influenced by tides, winds, waves, and a range of oceanographic processes (George et al., 2020; Chaudhuri et al., 2021; Prakash et al., 2021). This area plays a critical role in maintaining coastal water quality, facilitating ecological connectivity, and governing the transport of sediment and heat (Kumar et al., 2021). Tidal currents are particularly important in this region, contributing significantly to sediment transport, nutrient mixing, and the overall health of marine habitats on the inner shelf (Rivonker et al., 2018; Mazumdar, 2020; Mitra et al., 2022). Their impact on sediment dynamics along the Goa coast underscores the importance of accurate measurement and modeling to predict changes in coastal morphology (Kunte et al., 2002; Seelam et al., 2014).

Both low-frequency and high-frequency variability in ocean currents have been extensively studied on the continental shelf and slope of the west coast of India using observations and numerical models (for example, Shetye et al., 2008; Amol et al., 2018). Numerous studies have also focused on the characteristics of tidal currents in these regions, employing in situ measurements and modeling approaches (Shenoi et al., 1992; Subeesh et al., 2013; Subeesh and Unnikrishnan, 2016; Testut and Unnikrishnan, 2016; Subeesh et al., 2021). However, to the best of our knowledge, tidal current variability across the inner shelf and surf zone regions along the west coast of India has not been examined in detail. Most existing research on tidal dynamics in Indian coastal waters has focused on the continental shelf, slope, or estuarine systems, leaving a notable gap in understanding the tidal behavior across the surf zone and inner shelf. Additionally, the inner shelf and adjacent coastal region of the west coast of India may be strongly influenced by land-sea breeze systems, which may significantly affect current variability within the tidal frequency band. Despite this, as far as our best knowledge no studies to date have explored this influence in detail. In this study we seek to address these gaps by providing a detailed analysis of the spatial and temporal variability of barotropic currents in semidiurnal and diurnal bands in the inner shelf region and surf zone, based on both observations and numerical modeling.

The paper is organized as follows: Section 2 provides an overview of the study area, velocity observations in the surf zone and inner shelf, the model employed in this research, and a detailed description of the methodology. Section 3 presents the results, in which the first section describes the observation of barotropic currents, winds, and tides in the inner shelf and surf zone, and the second section focuses on semidiurnal and diurnal bands of barotropic currents. The model run and its sensitivity to various parameters are discussed in the next section. The model results are further utilised to examine the tidal characteristics, diurnal variation in currents, and the effect of wind on these semidiurnal and diurnal bands. Section 4 summarizes and concludes the paper.

2. Study area, observations and model

2.1 Study area

Goa has a coastline of about 105 km, composed of alternately situated headlands, estuaries, bays, and world-famous beaches situated on the central west coast of India. Goa state covers a stretch of 7 km of beach between Sinquerim/Candolim (15°30′37.00′′N; 73°45′51.00′′E) beach in the south and Calangute (15°32′55.00′′N; 73°45′10.00′′E) and Baga beach in the north (15°33′28.80′′N; 73°44′59.00′′E) (Figure 1a). The study regions, off Calangute and Candolim, are of significant interest due to its high incidence of surf zone injuries primarily due to rip currents and its socio-economic and environmental impacts (Venkateswarlu et al., 2023). Goa experiences a tropical, humid climate. It receives rainfall from the southwest monsoon winds from June to September. The annual rainfall ranges from 250 to 300 cm. The temperature in the region varies between 20° and 37°C.

2.2 ADCP and current meter observations

This study used data from the inner shelf (P1 in Figure 1) region off Goa (15°32′08.5′′N, 073°43′04.5′′E) from a bottom-looking Teledyne Acoustic Doppler Current Profiler (ADCP) operating at 614.4 kHz (Figure 1). The instrument was configured to record current components at 1 m intervals for depths ranging from 2 to 15 m. The measurements were conducted continuously from 11th January to 8th February 2017, in the inner shelf. The recorded data were processed using the WINADCP software after being internally stored as a temporal average at 10-minute intervals. The accuracy and quality checks of the data were performed during processing, such as evaluations of error velocity and the proportion of good data. Based on that, data from depths of 2–13 m were used in this study. The AANDERAA water level recorder (WLR) was also positioned at a depth of roughly 13 meters (P2 in Figure 1) close to ADCP during

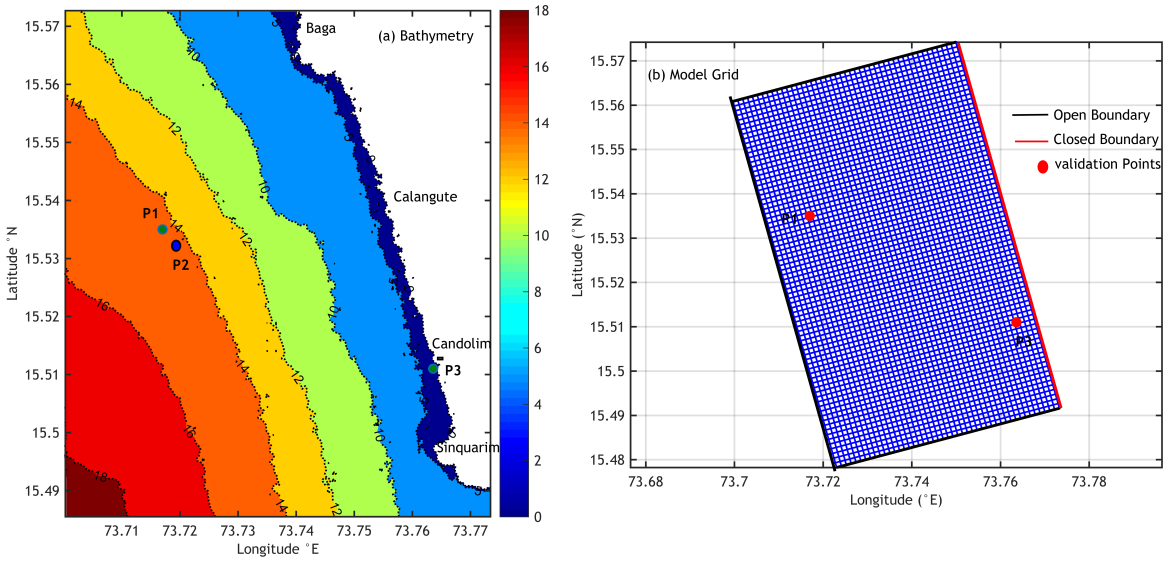

Figure 1. Topographic map of the study region with bathymetry contours at 5 m, 10 m, 12 m, 14 m, and 16 m (a). Bathymetry is also represented by color shading. Mooring sites are marked with filled circles: ADCP at P1, WLR at P2, and RCM9 at P3. Computational grid used in the DELFT3D model (b). The black line indicates the open boundary, the red line indicates the closed boundary, and measurement points of currents are shown as yellow circles (P1: ADCP, P3: RCM9).

this period. Additionally, at the inner surf zone (P3) of Candolim (15°30′38.13′′N, 73°45′51.26′′E), an AANDERAA Recording Current Meter-9 (RCM9) was also deployed at a water depth of 1.2 m for a period of 5 days from 19 th January to 25th January 2017. The ADCP measurement at inner shelf location "P1" (off Calangute) was about 7 kilometers northwest of the surf zone measurement location "P3" at Candolim. Apart from this, sea level data from a radar gauge installed by CSIR–NIO at Dona Paula Jetty, located at the northward mouth of the Zuari Estuary in Goa, India, were also utilized. The radar gauge data were averaged over a 5-minute interval referenced to chart datum (Mehra et al., 2013).

2.3 Numerical model Delft3D

In this study, a hydrodynamic model, Delft3D, developed by Deltares, was used to simulate the barotropic currents. Delft3D-Flow solves the Navier-Stokes equations for an incompressible fluid under shallow water and the Boussinesq assumptions (Stelling and Van Kester, 1994). The vertical accelerations were neglected by assuming they were small compared to the gravitational acceleration, therefore reducing the vertical momentum equation to the hydrostatic pressure equation. Delft3D-FLOW solves two-dimensional (2DH, depth-averaged) and three-dimensional (3D) unsteady flow and transport phenomena resulting from tidal, wave-driven, and density-driven forces. In this study, water was considered to be vertically homogeneous; hence, a depth-averaged approach was implemented (Luijendijk, 2001).

The model implemented for this study was very similar to the earlier setting by Yadhunath et al. (2022a), where the model was forced with the tide, wind, and wave inputs. A brief description of this environment is provided below. The model domain extended within two promontories on an 8 km long stretch of Goa beach between Sinquerim at the south and Baga at the northern end (Figure 1a). The structured rectangular grid were used to set the model domain, as shown in Figure 1, with a uniform horizontal grid resolution of 117 m (Figure 1b). The bathymetry for the model domain was taken from the NHO chart issued by Goa Port Trust and the measured bathymetry from the surf zone and intertidal regions by Yadhunath et al. (2022a). RFGRID and QUICKIN modules of Delft3D were used to create the grid and bathymetry for the model domain.

We used the one-month tidal elevation data measured from the Dona Paula Jetty (Figure 2b) to force the model along the open boundaries. Prior to this, we compared the tide at Dona Paula Jetty with the inner shelf tide and found that the tidal amplitude varied a little between these two locations (Supplementary Material). Hence, it was sensible to use the tidal elevation from the shallow jetty to force the boundary in the inner shelf. Measured wind at P1 using AWS (Automatic Weather station) was used as atmospheric forcing, and wave parameters at open boundaries were given from measurements at the inner shelf. The coupled flow and wave module was used to incorporate waves in the model. The roughness formula used was Chezy, and the roughness values for the cross-shore (V)

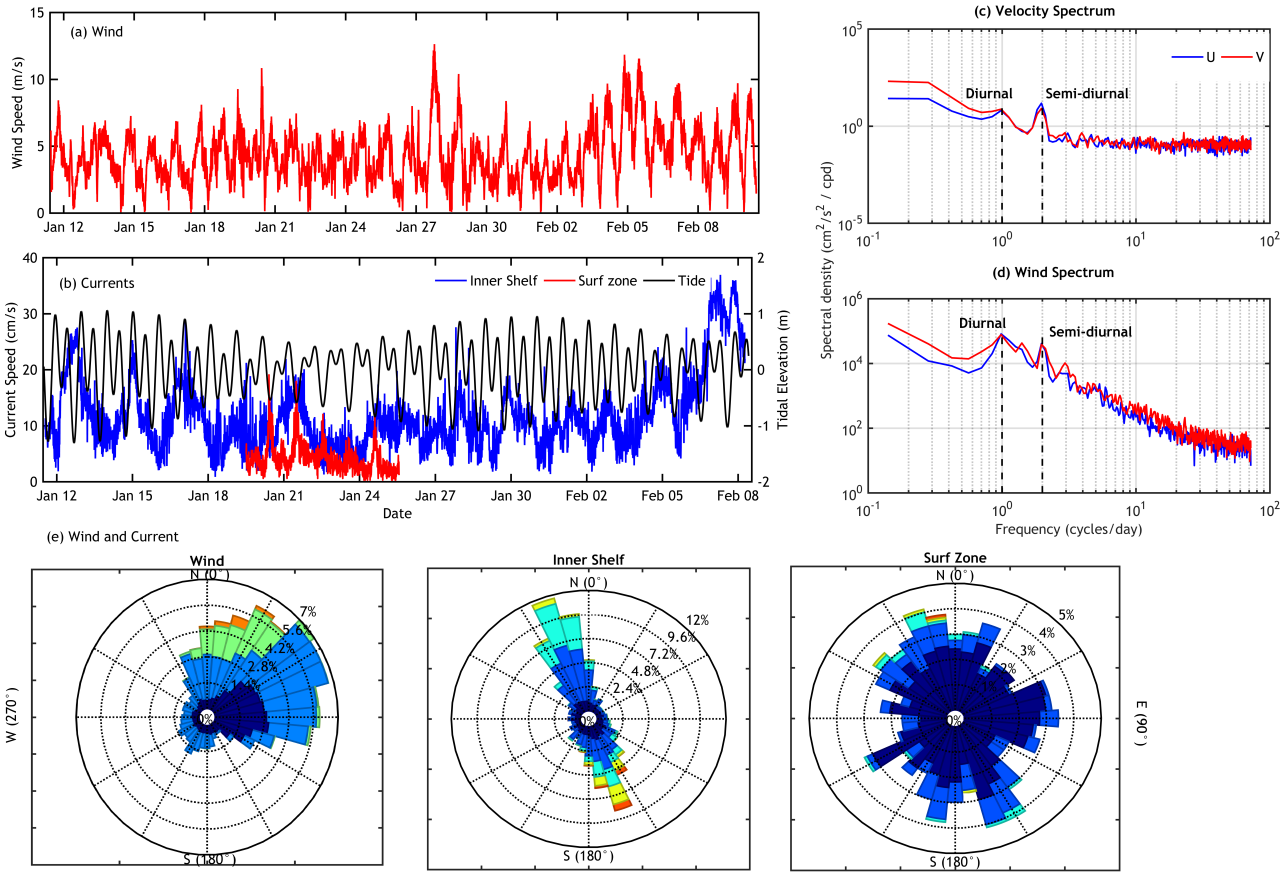

Figure 2. Time series of measured wind speed at inner shelf (a). Measured current speed at inner shelf and surf zone with tidal elevation (black line) at inner shelf (b). The scale of current speed is given in lhs and scale of tidal elevation is given in rhs. Power spectral density of barotropic currents (c), wind speed at inner shelf (d). The eastward component is represented by blue and the northward component is represented by red. Semidiurnal and diurnal frequencies are marked as vertical dashed lines. Rose diagram of measured wind direction, current direction at P1, and current direction at Surf zone (e).

and along-shore (U) components were taken as 30 $ms^{-1/2}$. A sensitivity study was undertaken to identify the role of physical parameters and roughness on model performance. Optimum settings were selected by comparing the barotropic currents with that of the inner shelf and surf zone. The details of sensitivity experiments are given in section 3.2.1. Model performance was evaluated using statistical metrics including Index of Agreement (IA), bias, RMSD, and R^2 for both velocity components.

2.4 Methods

Barotropic current at the inner shelf was computed by vertical averaging of total currents (Subeesh et al., 2013). This method was sensible, as the ADCP data covers more than 70% of the water column here. Currents at the surf zone are considered as barotropic. Barotropic currents from the inner shelf and surf zone were then subjected to harmonic analysis to extract tidal currents. The three major semidiurnal components, M2, S2, and N2, as well as the two diurnal components, K1 and O1, were extracted. Higher harmonics are found negligible and not considered for analysis. The relationship between the eastward and northward components of tidal currents is described by the tidal ellipse parameters. Additionally, harmonic analysis was carried out on WLR data and radar gauge data installed at the Dona Paula Jetty to extract the tidal elevation.

3. Results

3.1 Observations

3.1.1 Wind, tides and barotropic currents

The time series data for wind, tides, and barotropic currents from the inner shelf and surf zone are presented. Figure 2a shows the time series of wind measurements from the inner shelf. Mostly wind speeds remain below 10 m/s, with a maximum recorded value of 15 m/s. The temporal mean wind speed is 5 m/s. A gradual increase in

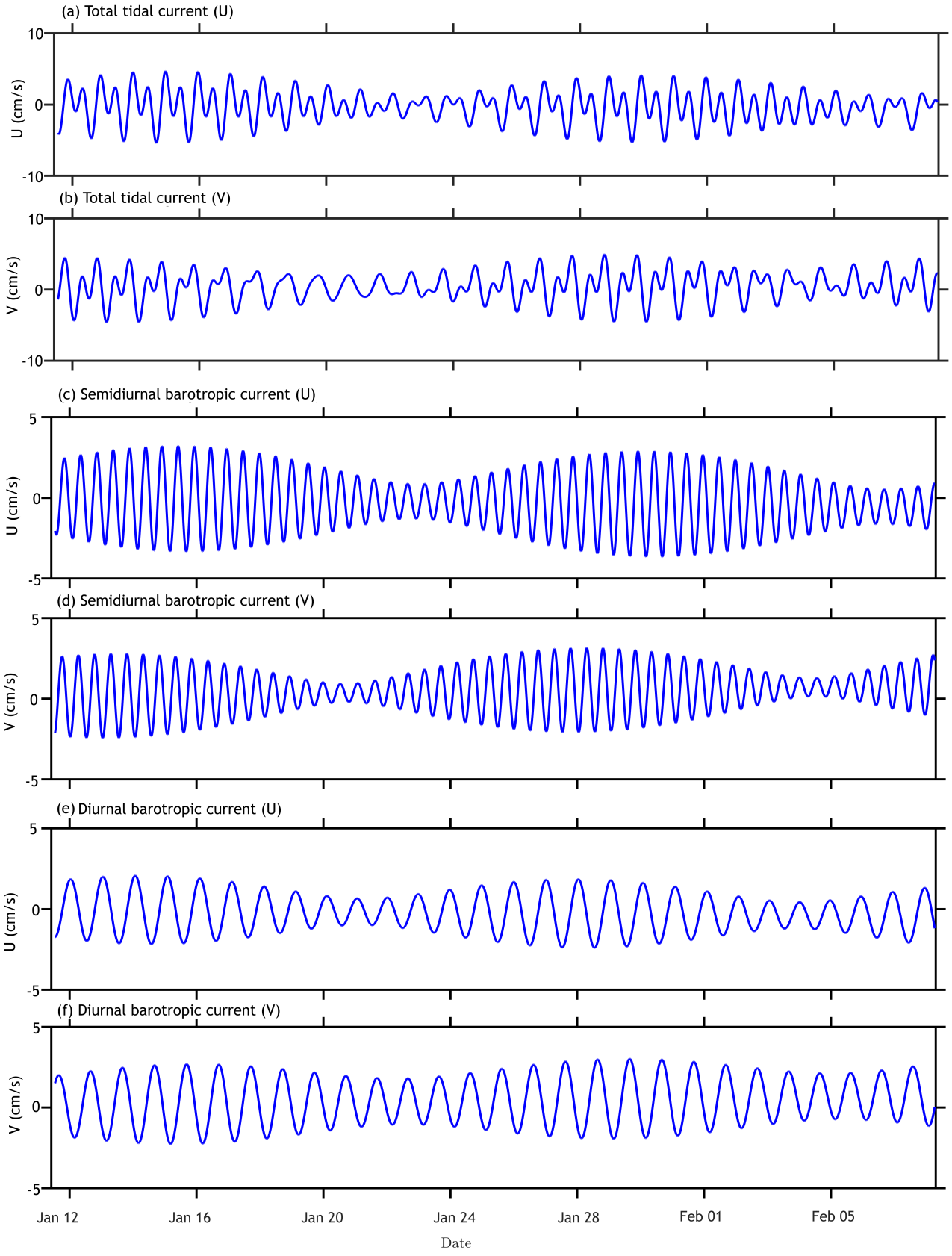

Figure 3. Time series of total barotropic and tidal current components measured at the inner shelf. Panels (a) and (b) show the total barotropic U- and V-velocity components, respectively; (c) and (d) show the semi-diurnal U and V components; and (e) and (f) show the diurnal U and V components.

wind magnitude is observed from February 1st to February 6th. The rose diagram shows that the prevailing wind direction is from the northeast (Figure 2e), likely reflecting the climatological wind patterns associated with the northeast monsoon in theregion.

Observations of barotropic currents from the inner shelf and surf zone locations, along with the tidal elevation at the inner shelf, are shown in Figure 2b. Tidal range is lower than 2 m, and a clear spring-neap cycle is evident in the observation. Detailed analysis of tides at the inner shelf and Jetty are given in Supplementary Material. Compared to the inner shelf, currents are relatively weaker in the surf zone during this observation period. The average speed observed at the surf zone was ∼4 cm/s, whereas at the inner shelf it is ∼9 cm/s. The maximum current speed at the surf zone is 19 cm/s, whereas at the inner shelf it is 22 cm/s. The current speed in the surf zone reaches its peak during the ebb phase, indicating that it is significantly higher when the tidal range is at its maximum (Yadhunath et al., 2022b). On the inner shelf, although stronger currents occurred during the low tidal phase, there is no clear relationship between maximum tidal range and peak current speed (Figure 2b). A rose diagram of measured current at the inner shelf location and surf zone is shown in Figure 2e. In the inner shelf the currents are predominantly towards the southeast and northwest directions, i.e., parallel to the isobath. The cross-isobath component is relatively weak. In the surf zone, the current direction is predominantly between the southwest and northwest.

Figure 2c and 2d show the power spectra of both barotropic currents and wind. At the inner shelf spectra were computed using one-month data. Power spectral density was estimated using the Welch method with 50% overlapping with a Hamming window of 256 data points. Both barotropic currents and wind show peaks in semidiurnal and diurnal frequency bands. In barotropic current velocity spectra, semidiurnal frequency dominates over diurnal frequency. In winds, diurnal frequency bands show higher energy compared to semidiurnal bands. The dominance of diurnal bands in wind may be due to the land-sea breeze in the region. The diurnal and semidiurnal bands in the currents will be discussed in section 3.1.2.

3.1.2 Barotropic tidal currents in the inner shelf

As a next step, we extracted barotropic currents in the tidal band from the inner shelf ADCP observation. It is noted that the eastward component of tidal current is stronger compared to the northward component, indicating the predominant cross-shelf flow of tides. Maximum eastward velocity observed is approximately 9 cm/s. A spring-neap cycle is observed in the currents, as noted in tidal elevation (Figure 3).

Time series of barotropic tidal currents show that the tides are mixed semidiurnal. Hence, we analyzed semidiurnal and diurnal barotropic tidal currents separately. To extract semidiurnal (diurnal) tidal currents, the M2, S2, and N2 (K1 and O1) constituents are retained, and harmonic analysis were performed. The time series of both bands are shown (Figure 3c–f). Semidiurnal barotropic tides are relatively stronger compared to diurnal. In both bands, the eastward component is larger compared to the northward component. The spring-neap cycle is more evident in the semidiurnal band compared to the diurnal. The spring-neap cycle follows a more or less similar phase in both bands. In the semidiurnal band, the M2 constituent is the largest over the inner shelf, followed by S2 and N2. In the diurnal band, the largest constituent is K1, followed by O1. The K1 and S2 amplitudes are in a nearly comparable range, but O1 is the weakest constituent (Table 1).

Table 1. Barotropic tidal ellipse parameter for major tidal constituents M2, S2, N2, K1, and O1.

Constituents	Semi-major [cm s^{-1}]	Semi-minor [cm s^{-1}]	Angle [°]	Phase [°]
M2	2.55	0.78	34.47	35.94
S2	1.11	1.06	−1.18	90.11
N2	0.57	0.07	70.55	−20.84
K1	2.59	0.97	−54.47	137.52
O1	1.02	0.09	−38.73	−190.15

Tidal ellipse parameters were derived from the amplitude and phase of the eastward and northward components of the tidal constituents (Table 1). The semi-major axes of the M2 and K1 constituents exhibit similar amplitudes, with values of 2.55 cm/s and 2.59 cm/s, respectively. Despite their comparable magnitudes, the orientation of the tidal ellipses differs: semidiurnal tides (M2, N2) tend to propagate more across-isobath, whereas diurnal tides (K1, O1) are predominantly aligned along-isobath. The S2 constituent, the second most energetic semidiurnal component, exhibits a more circular shape, characterized by nearly equal semi-major and semi-minor axes.

3.1.3 Barotropic currents in diurnal and semidiurnal bands in the surf zone

A five-day observation of currents at the depth of 1.2 m during the neap phase of the tidal cycle was used to understand the barotropic currents in the semidiurnal and diurnal band in the surf zone. Since the five-day time series was insufficient to separate individual tidal components, we used a second order band pass Butterworth filter to separate the semidiurnal and diurnal current in the surf zone. The eastward component exhibits a maximum amplitude of 2.8 cm/s, while the northward component reaches a peak amplitude of 4.5 cm/s. And the northward component predominates during the ebb tide, while the eastward component follows the tidal oscillations, peaking during the flood tide period.

In the semidiurnal band, the eastward current is stronger than the northward with a peak amplitude of 1.7 cm/s (Figure 4c). Initially, the eastward current in the surf zone is

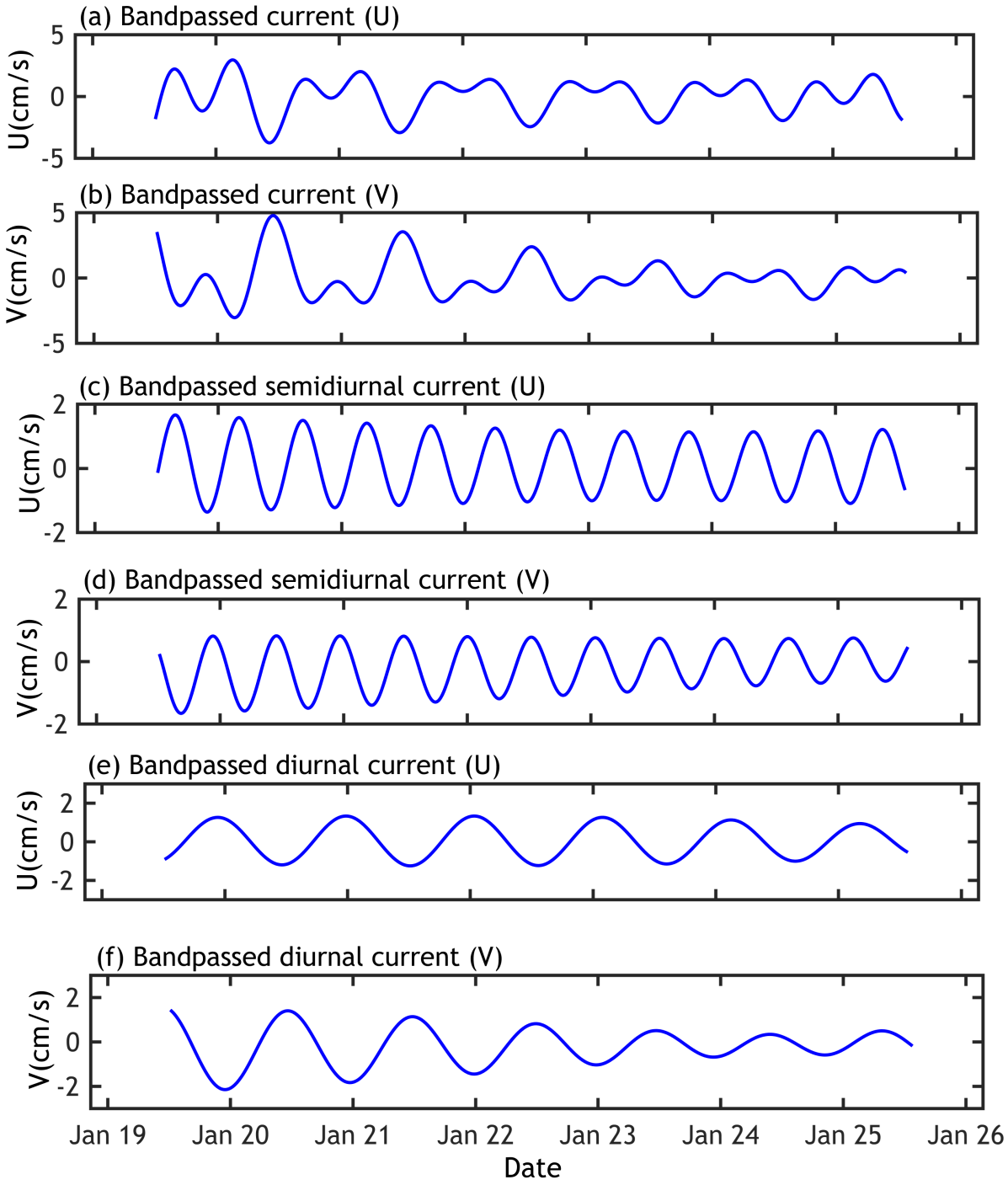

Figure 4. Time series of total barotropic and tidal current components measured at the surf zone. Panels (a) and (b) show the total barotropic U- and V-velocity components, respectively; (c) and (d) shows the semi-diurnal U and V components; and (e) and (f) show the diurnal U and V components.

weaker than that on the inner shelf for a few tidal phases, but its strength increases over time, and amplitudes eventually aligns with inner shelf currents. However, the northward current is much stronger in the surf zone initially for a few tidal cycles, while its amplitude decreases compared to the inner shelf (Figure 4d).

On the other hand, the diurnal variability at the surf zone inferred that the eastward component is almost as strong as the inner shelf, with an amplitude of 1.30 cm/s (Figure 4d). The northward component is relatively strong during the initial tidal phases, with amplitudes up to 2.0 cm/s, but later weakens as the inner shelf currents be-

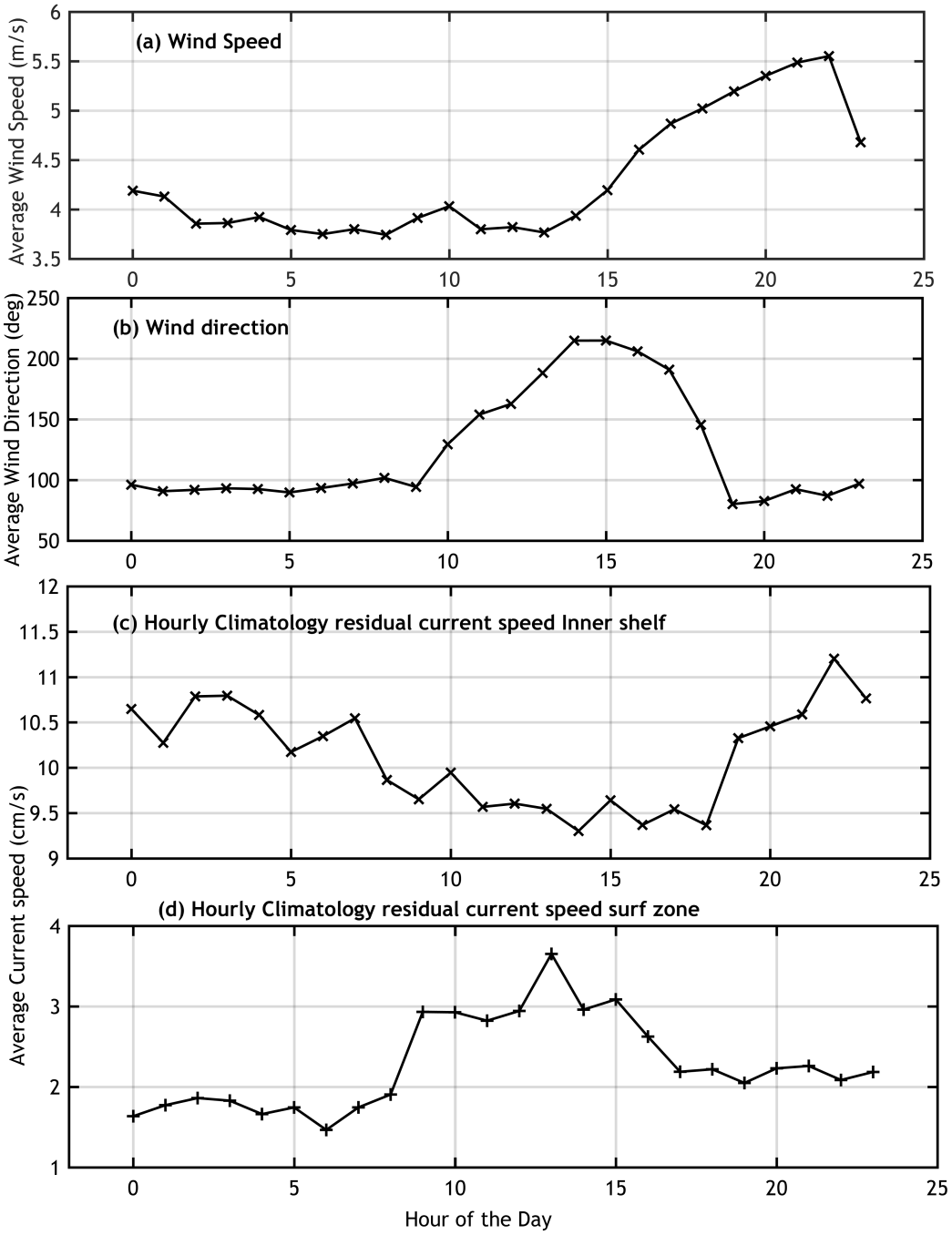

Figure 5. Observed hourly climatology of wind speed (a), wind direction (b), and current speed (c) in the inner shelf, along with hourly climatology of residual current speed in the Surf zone (d).

come dominant. In this meso-tidal region, the currents are considerably stronger than expected from tidal forcing alone, suggesting additional influence from local wind and wave effects. In the semidiurnal band, a reduction in tidal current amplitude is observes between 22 and 24 January, coinciding with a similar decline in the prevailing wind components. The role of wind forcing in modulating semidiurnal and diurnal barotropic currents in the surf zone is examined in detail through numerical model simulations (section 3.2).

Table 2. Model sensitivity experiment with different model sensitivity parameters.

Parameter	Sub parameter	R1	R2	R3	R4	R5	R6	R7	R8	R9	R10
Roughness formulae	Chezy	30/30	40/40	30/30	30/30	65/65	Spatially varying	Spatially varying	Spatially varying	Spatially varying	Spatially varying
Physical processes	Wave	N	N	N	N	Y	N	N	Y	N	N
	Wind	Y	Y	Y	Y	Y	Y	Y	Y	N	Y
Wind drag coefficients	A	0.0045	0.0045	0.0006	0.0006	0.0006	0.0006	0.0006	0.0006	N	0.0006
	B	0.0055	0.0055	0.0015	0.0015	0.0015	0.0015	0.0015	0.0015	N	0.0015
	C	0.0055	0.0055	0.0015	0.0015	0.0015	0.0015	0.0015	0.0015	N	0.0015
Open boundary conditions	North	WL	WL	WL	Neumann	Neumann	Neumann	Neumann	Neumann	Neumann	N
	South	WL	WL	WL	WL	WL	Neumann	WL	WL	WL	N
	West	WL	WL	WL	WL	WL	WL	WL	WL	WL	N
Index of agreement (IA)	U	0.65	0.65	0.7	0.76	0.66	0.76	0.77	0.79	0.71	0.12
	V	0.40	0.53	0.38	0.63	0.58	0.47	0.69	0.66	0.38	0.14
bias	U	0.24	0.22	0.25	0.21	0.11	0.27	0.17	0.18	0.25	0.25
	V	−0.35	−0.34	−0.41	−0.31	−0.13	−0.41	−0.26	−0.27	−0.43	−0.43
RMSD	U	1.82	1.63	1.51	1.07	1.52	0.96	0.96	0.92	1.11	2.15
	V	2.48	2.09	2.44	1.25	1.71	1.58	1.13	1.2	1.65	2.17
R2	U	0.85	0.82	0.88	0.88	0.78	0.90	0.90	0.91	0.87	−0.55
	V	0.22	0.48	0.17	0.82	0.65	0.74	0.86	0.84	0.81	−0.37

3.1.4 Diurnal variability of barotropic currents

To examine diurnal variability of barotropic currents, an hourly climatology was computed using one-month velocity data on the inner shelf. The tidal component was removed from the time series before computing climatology. Results show that average current speeds are notably higher at nighttime compared to daytime (Figure 5a). Measurements of wind speed reveal that winds are generally stronger (5.5 m/s) at night than they are during the day (Figure 5d), indicating the possible role of strong winds on strong currents during nighttime.

We next analyse the hourly climatology of surf zone currents. Results show that, unlike on the inner shelf, daytime currents are stronger than night time currents in the surf zone, even in the presence of strong night time winds. The wave parameters, beach slope, and local bathymetry are the potential factors that control the current's speed in the surf zone (Basco, 1983). To understand the role of wave parameters in the diurnal variation of surf zone currents, the hourly climatology of measured significant wave height (Hs) and wave direction from the surf zone during this period is analysed. The Hs shows significant variability with higher amplitudes at nighttime. The increase in the nighttime wind may be the reason for the high amplitude of waves during this period. However, this relation is not clear during the morning time, when the Hs is large even when the winds are weak, indicating the presence of remotely forced waves.

The relationship between surf zone currents and Hs is not direct. Hourly climatology reveals that surf zone currents peak between 09:00 and 15:00 hours. Although Hs exhibits an increasing trend during this period, the maxima of current velocity and Hs do not coincide (Figure 4). Instead, a distinct shift in wave propagation angle is observed during the peak current period, with waves approaching more obliquely from the southwest. This combination of elevated Hs and a change in wave direction is likely a contributing factor to the daytime intensification of surf zone currents. It should be noted that the climatology is based on a 5-day dataset, which may not fully capture the variability of surf zone currents in the region. To further investigate the influence of wave parameters on surf zone currents, we will utilize model simulations in section 3.2.5.

3.2 Numerical modelling Delft3D

3.2.1 Model sensitivity

Various sensitivity experiments (Table 1) were carried out to identify the optimum setting for the model to reproduce barotropic currents in the inner shelf and surf zone. Statistical parameters, including Index of Agreement (IA), bias, RMSD, and R^2 for both the U and V barotropic velocity at mooring locations, are computed for each experiment (Table 2). The simulation of barotropic currents showed sensitivity to Chezy roughness, boundary condi-

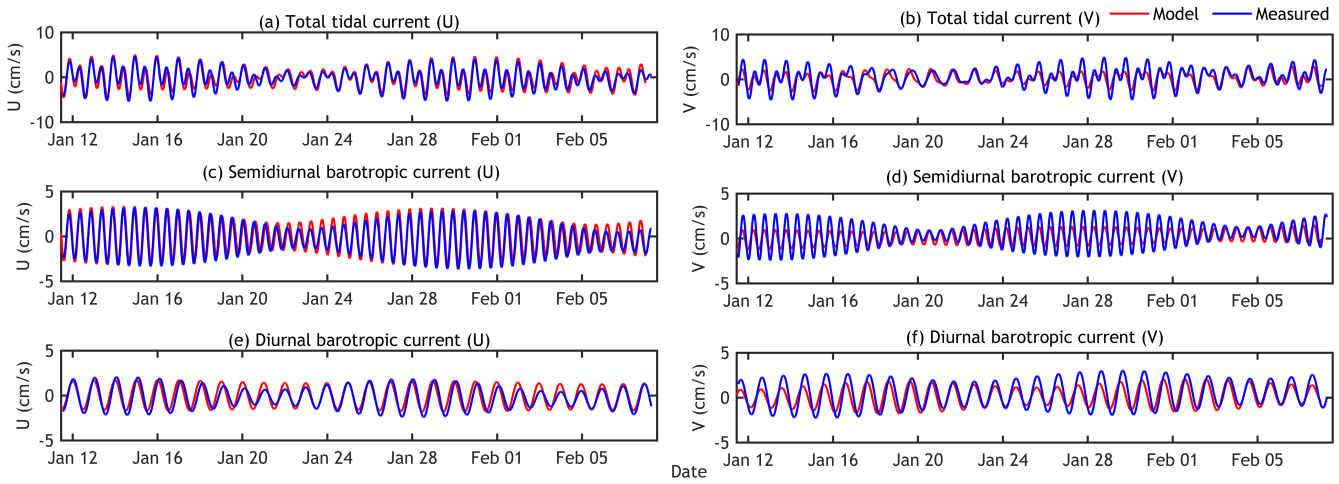

Figure 6. Time series comparison between modelled and observed currents at tidal bands in the inner shelf. Panels (a) and (b) present the total barotropic tidal currents for U and V components; (c) and (d) depict the semidiurnal U and V components; and (e) and (f) depict the diurnal U and V components.

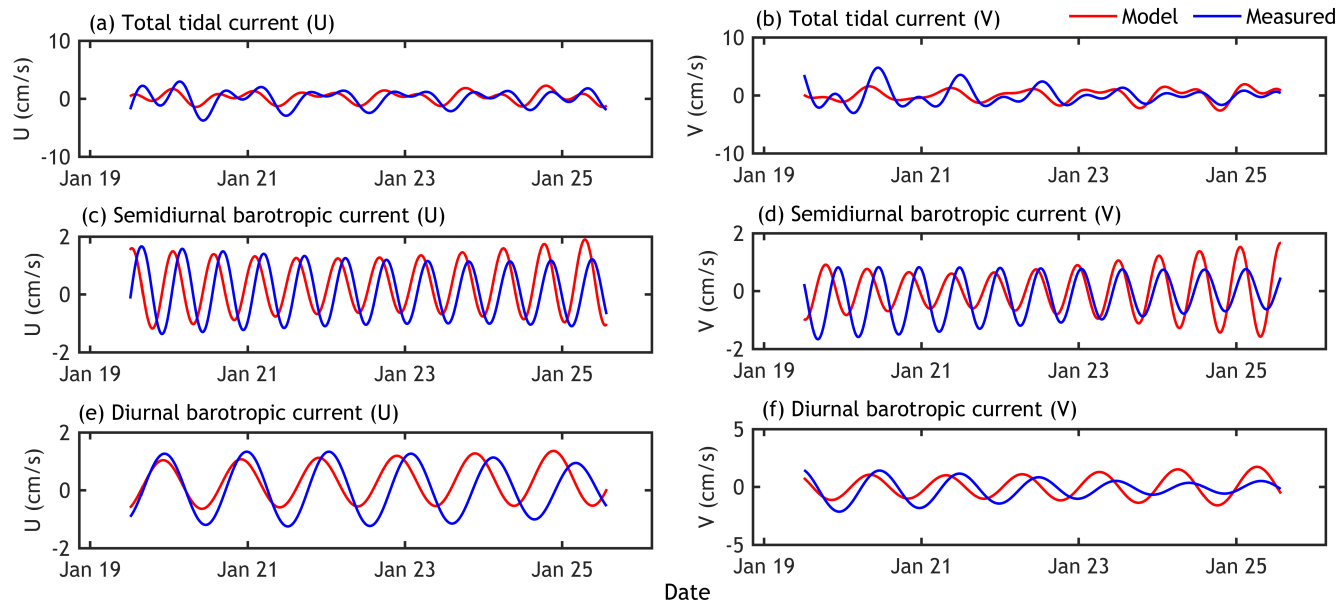

Figure 7. Time series comparison of model and measured total barotropic and tidal current components at the Surf zone. Panels (a) and (b) show the total barotropic U- and V-velocity components, respectively; (c) and (d) show the semi-diurnal U and V components; and (e) and (f) show the diurnal U and V components.

tions, and forcing parameters. Using a uniform Chezy of 30 m $s^{-1/2}$ yielded poor performance, particularly for the v-component (RMSD = 2.48 cm s^{-1}). Increasing Chezy to 40 m $s^{-1/2}$ improved correlation, but RMSD remained high. Implementing low wind drag coefficients and Neumann boundaries (R4–R5) enhanced correlations, while wave forcing with high Chezy overdamped currents. Introducing spatially varying Chezy with appropriate northern and southern boundary conditions (R6–R7) substantially improved correlations (U = 0.90, V = 0.74), but improvements are needed in RMSD and bias. To achieve a physically realistic representation of coastal currents, wave forcing was incorporated, which further reduced RMSD and enhanced correlation (U = 0.91, V = 0.84). Sensitivity experiments confirmed that spatially varying roughness and combined wave-wind forcing are critical for accurately simulating barotropic currents in this region, while proper boundary specification is essential for model sta-

Table 3. Comparison between amplitudes and phases of barotropic U and V components measured from P1 using ADCP with the model.

	Amplitude [cm/s]		Phase [°]			
U components	Measured	Modelled	Measured	Modelled	Amplitude Diff.	Phase Diff. [°]
M2	2.15	2.33	238.00	258.00	−0.18	−20
S2	1.11	0.83	306.00	301.00	0.28	5
N2	0.20	0.48	198.00	230.00	−0.28	−32
K1	1.70	1.72	046.10	027.30	−0.02	−18.8
O1	0.80	0.12	324.00	244.00	0.68	80
	Amplitude [cm/s]		Phase [°]			
V components	Measured	Modelled	Measured	Modelled	Amplitude Diff.	Phase Diff. [°]
M2	1.58	0.94	202.00	188.00	0.64	14
S2	1.06	0.24	215.00	168.00	0.82	47
N2	0.54	0.40	219.00	163.00	0.14	56
K1	2.18	1.59	269.00	247.00	0.59	22
O1	0.64	0.54	154.00	58.00	0.10	96.

bility. Based on these findings, subsequent analyses focus on the R8 configuration with wave, wind, and water level forcing.

3.2.2 Model comparison in the inner shelf and surf zone

We next compare the simulated tidal currents at the inner shelf with observations. The eastward and northward components of barotropic tidal currents from both observation and model are shown in Figure 6. The model shows a good correlation with observation in the eastward component with a value of 0.91 and 0.84 for the northward component. The RMSD is relatively small for the eastward component (approximately 0.92 cm/s) and 1.2 cm/s for northward, despite the bias being positive for the eastward component (0.18) and negative for the northward component (−0.27). The high correlation and low RMSD indicate that the model captures the tidal currents quite well, especially in the eastward direction. The small bias in each component indicates a minor error (slight overestimation in eastward, slight underestimation in northward), but this is modest relative to the overall error magnitude.

Harmonic analysis of model-simulated eastward currents shows that the M2 tidal constituent has the largest amplitude, followed by K1 and S2 (Table 3). O1 is the weakest tidal constituent in the eastward component. This is similar to the observations. The amplitude difference between the measured constituents and the model was found to be within the range of 0.7 cm/s differences. The phase difference of O1 is somewhat high when compared to the results of the remaining constituents, which are nearly in phase with the measurements. In the case of the northward component, the model predicted that the weakest constituent is S2 and the strongest is the diurnal component K1, followed by M2, O1, and N2. When comparing the model and measurements, the phase difference is significantly larger, especially for the N2 and O1 components, even though the amplitude differences of these components are less than 0.2 cm/s (Table 3).

Barotropic currents extracted from the model simulation were compared with surf zone observations. The model fails to reproduce currents in the tidal band more accurately, like the inner shelf in the surf zone, where its performance is relatively poor. To evaluate the model's ability to simulate the semidiurnal and diurnal bands, the simulated currents were compared with observations at these frequencies. In the surf zone, the model predicted barotropic currents with a correlation of 0.48 and an RMSD of 1.24 cm/s for the eastward component and a correlation of 0.46 with an RMSD of 1.3 cm/s for the northward component (Figure 7a,b). In both the semidiurnal and diurnal bands, the model slightly overestimated the current amplitudes, and a noticeable phase shift was observed relative to the measurements.

3.2.3 Spatial characteristics of tidal currents

Ellipse parameters estimated from the model and observation at the inner shelf is first compared (Table 4). The model successfully predicts the direction of propagation of tidal currents in the inner shelf region, closely aligning with the measured components. The model slightly underestimates the semi-major axis of the M2 constituent (2.35 cm/s) compared to the measured value (2.55 cm/s) and overestimates the semi-minor axis (0.88 cm/s modeled vs. 0.78 cm/s measured), while exhibiting a significant phase shift of 35°. For the K1 component, the model also slightly underestimates the semi-major axis (2.20 cm/s modeled vs. 2.59 cm/s measured) but shows a closer alignment in phase (140.22° modeled vs. 137.52° measured).

Figure 8 shows the spatial distribution of M2 and K1 ellipses in the inner shelf. The M2 ellipse of the tidal current shows that the current propagate in the cross-isobath direction. Whereas the diurnal component K1 propagates

Table 4. Barotropic tidal ellipse parameter comparison with model for major tidal constituents M2, S2, N2, K1, and O1.

Location: Inner shelf	Semi Major [cm s^{-1}]		Semi Minor [cm s^{-1}]		Angle [°]		Phase [°]	
Components	Measured	Model	Measured	Model	Measured	Model	Measured	Model
M2	2.55	2.35	0.78	0.88	34.47	9.13	35.94	70.10
S2	1.11	0.85	1.06	0.17	−1.18	−11.36	90.11	−227.19
N2	0.57	0.53	0.07	0.33	70.55	32.50	−20.84	−293.26
K1	2.59	2.20	0.97	0.79	−54.47	−41.91	137.52	140.22
O1	1.02	0.55	0.09	0.01	−38.73	−77.47	−190.15	−173.98

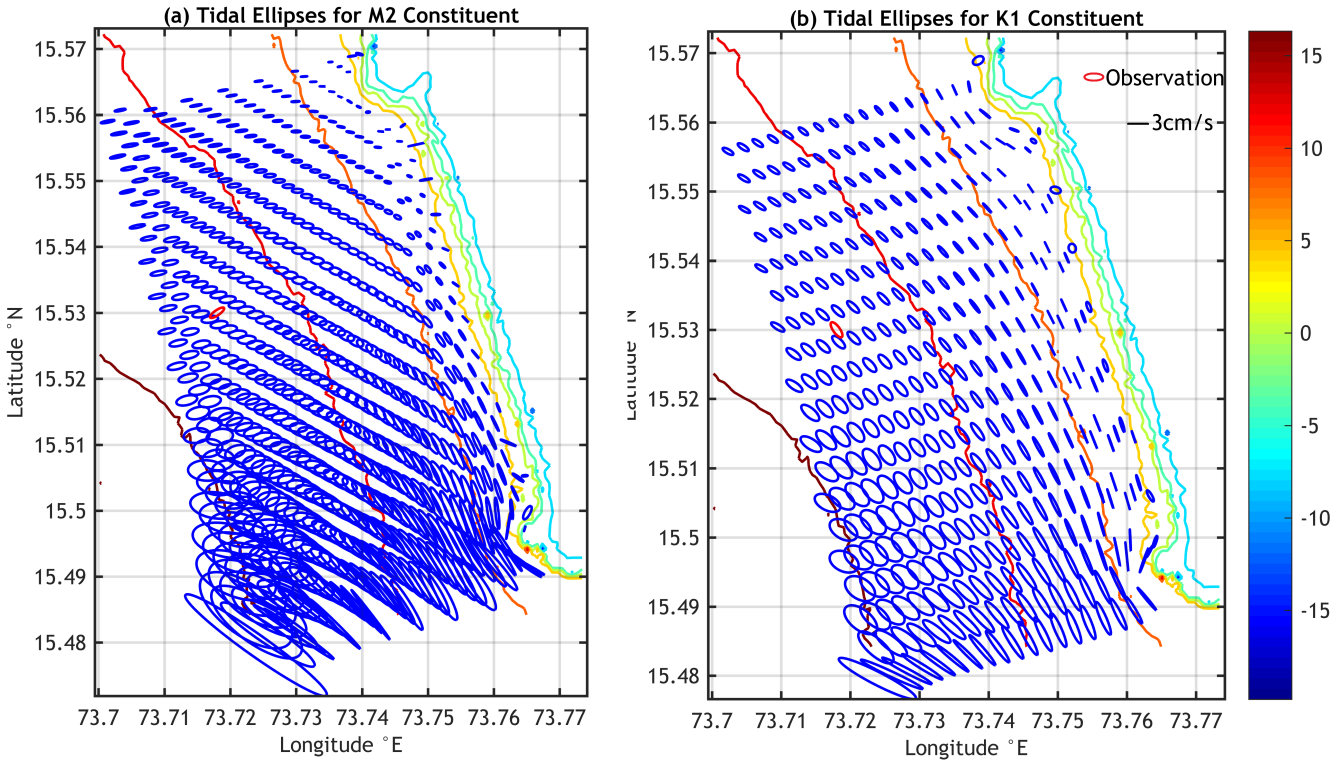

Figure 8. The spatial distribution of a) semi-diurnal (M2) and b) diurnal (K1) barotropic tidal ellipse (blue circle) from the model. The red circles represent the measured ellipse at P1.

along isobaths at the inner shelf. However, in the surf zone, both constituents show similar directions of propagation. But the magnitude of the semidiurnal component is only 2.55 cm/s, which is half of the observed magnitude at the continental shelf by Subeesh et al. (2013), and diurnal component K1 exhibits a magnitude of 2.59 cm/s.

3.2.4 Role of winds in semidiurnal and diurnal barotropic currents

Two model sensitivity experiments-one with tides only and another with winds only-were conducted to examine the influence of wind on barotropic currents in the semidiurnal and diurnal bands over the inner shelf and surf zone. Power spectra were calculated at each grid point using one-month model output from the two simulations. Figure 9 presents the spectra of the eastward and northward velocity components in the inner shelf and surf zone mooring locations. On the inner shelf, the tide-only run exhibits well-defined peaks in both semidiurnal and diurnal frequency bands (Figure 9a). In contrast, the wind-only run shows elevated energy in the diurnal band of the northward component, but without a distinct peak. These results suggest that winds play only a minimal role in driving semidiurnal and diurnal barotropic currents on the inner shelf. Within the surf zone, the tide-only simulation shows elevated spectral peaks in the semidiurnal band compared to the wind-only case (Figure 9b). Nevertheless, the presence of non-negligible energy in the semidiurnal band of the wind-only run points to the contribution of semidiurnal winds in driving semidiurnal barotropic currents. In the diurnal band, however, the wind-only simulation exhibits markedly higher energy than the tide-only run, highlighting the dominant influence of winds on diurnal

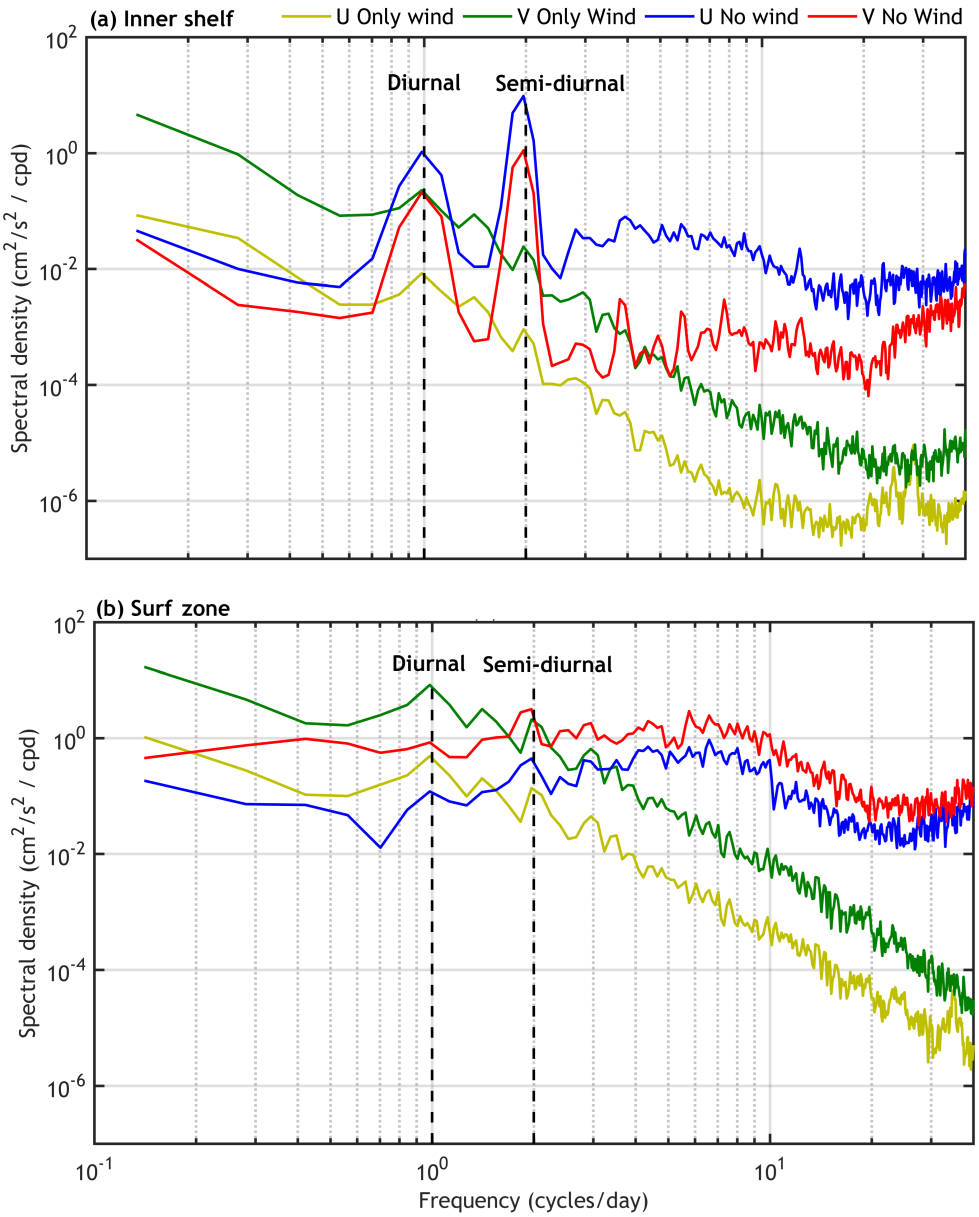

Figure 9. Power spectral density of the barotropic current components modelled at the (a) inner shelf and (b) surf zone with forcing wind alone and tide alone.

barotropic currents in the surf zone. To investigate the influence of wind on semidiurnal and diurnal barotropic currents within the model domain, the spatial distribution of band-averaged spectral energy from two simulations is presented in Figure 10. In the wind-only simulation, diurnal-band energy is broadly distributed across the surf zone (Figure 10c), whereas semidiurnal-band energy appears more localized, confined to discrete patches (Figure 10d). On the inner shelf, wind has a comparatively weaker effect on both semidiurnal and diurnal barotropic currents. To further quantify wind and current interaction, band-pass filtered time series were extracted for diurnal and semidiurnal frequency bands, and correlation coefficients and variance contribution rates were computed separately for the inner shelf and surf zone. On the inner shelf, correlations between diurnal wind and current components are moderate ($r = 0.44$ for U and $r = -0.61$ for V), while correlations for semidiurnal U and V are ranged from $r = 0.46$ to 0.64. These correspond to variance contributions of approximately 19–41%, indicating that wind exerts a secondary, modulating influence on tidal currents, with astronomical tides remaining the dominant forcing. Whereas at surf-zone currents exhibit markedly stronger wind-current coupling. The v-component shows

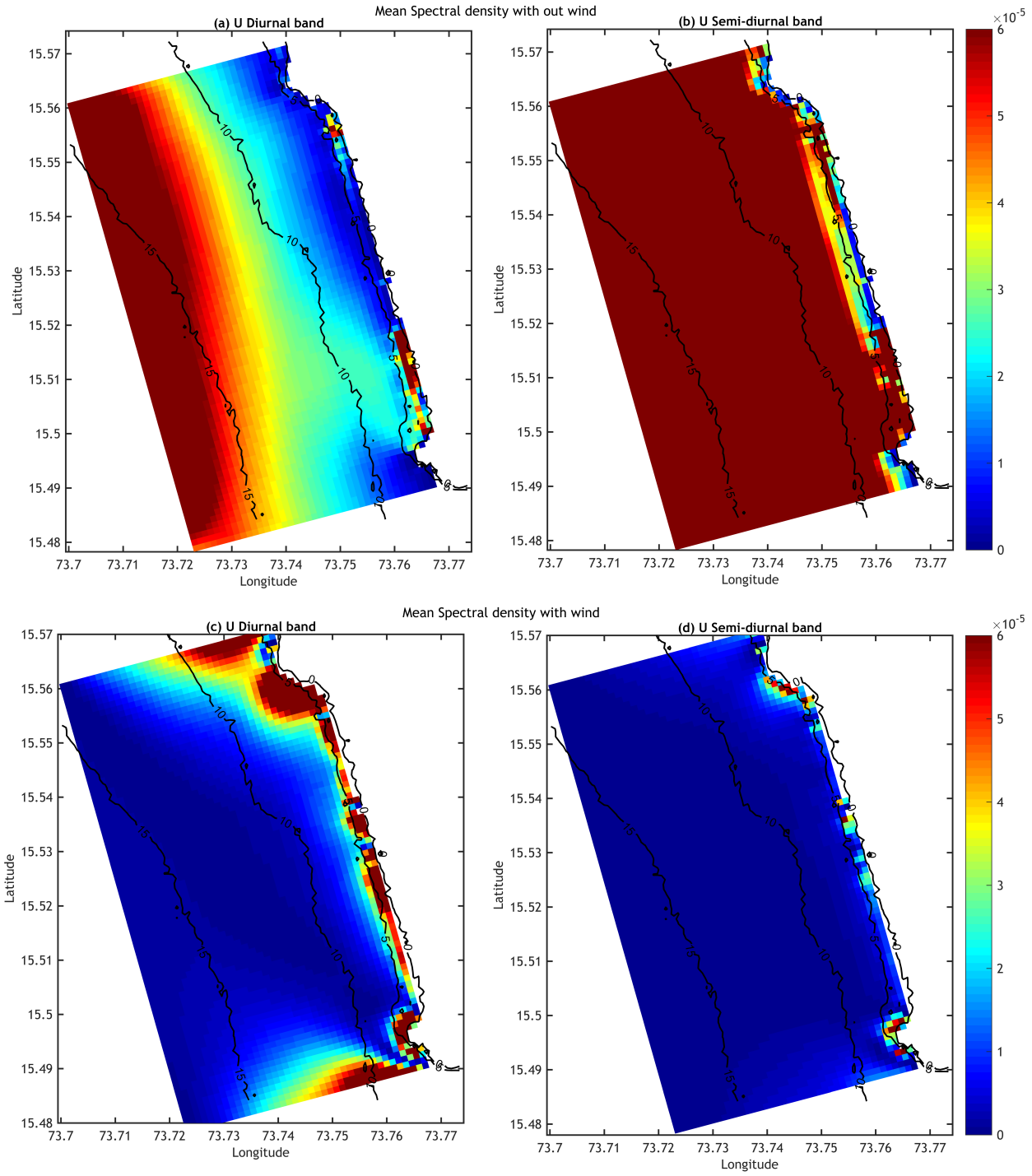

Figure 10. Power spectral density of the eastward barotropic current showing diurnal and semi-diurnal frequency bands under different forcing scenarios. Panels (a) and (b) correspond to spectra when the model is forced only by tide, while (c) and (d) correspond to spectra when forced only by wind.

very high correlations with wind at both diurnal ($r = 0.97$) and semidiurnal ($r = 0.93$) frequencies, explaining over 85% of the variance. The u-component displays weaker and partly anti-phase correlations, particularly at semidiurnal frequencies ($r = -0.52$).

3.2.5 Influence of waves in diurnal variability in surf zone

Observations indicate pronounced diurnal variability in surf zone currents, with maximum current speeds occurring during daytime hours. This variability is closely associated with changes in wave direction and wave amplitude

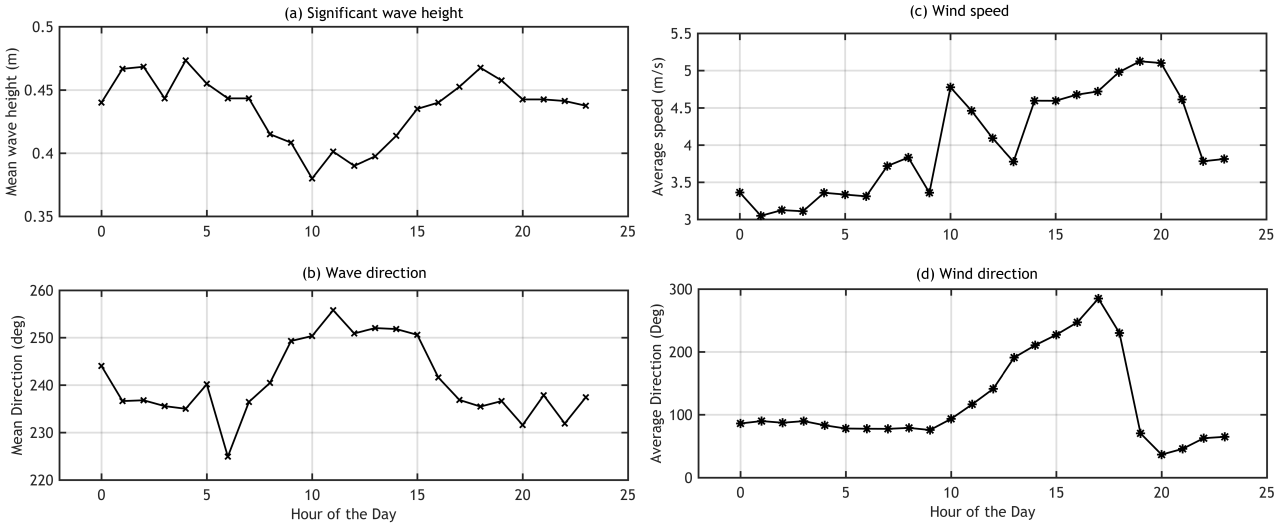

Figure 11. Hourly climatology of significant wave height (a) and mean wave direction (b) measured in the Surf zone, along with mean wind speed (c) and mean wind direction (d) during 19–25 January 2017.

(Figure 11a,b). To investigate the diurnal variability of barotropic currents in the surf zone and assess the roles of significant wave height and wave direction in this variability, hourly climatology from the model simulations at the surf zone location were analyzed. The model results show that wave height gradually increased from 00:00 to 12:00 hours, peaked around 15:00 hours, and subsequently declined. A similar diurnal pattern was evident in the residual current climatology, with current speeds increasing alongside wave height, reaching a maximum of 6.5 cm/s near midday, and decreasing thereafter. This daytime intensification of currents is well captured by the model and is consistent with observations. However, observations suggest that surf zone current variability is more strongly correlated with wave direction than with wave amplitude. In the model this relation is not well evident, as the wave direction is more or less similar in the model, which is coming from the southwest direction. Further, a sensitivity experiment with and without wave forcing was performed to understand the role of wave parameters in surf zone currents. A marked reduction in current magnitude is noted in the surf zone currents without wave forcing (Figure 12), indicating the importance of wave parameters in determining surf zone currents.

4. Discussion and conclusion

This study presents a comprehensive analysis of mooring observations of currents, winds, and tides in the shallow coastal waters off Goa. Spectral analysis reveals significant energy in both the semidiurnal and diurnal frequency bands for winds and currents in the inner shelf. The pronounced diurnal peak in the wind spectrum is likely associated with the land-sea breeze system, consistent with previous studies (Allouche et al., 2023). While the semidiurnal and diurnal peaks in barotropic currents are typically attributed to tidal forcing, the concurrent presence of wind energy in these bands highlights the need for a detailed examination of the influence of winds in these two bands. Understanding the relative contributions of tidal and wind forcing in these frequency bands is essential for accurately characterizing coastal dynamics in this region.

Tidal components of the currents in the inner shelf were extracted using harmonic analysis. Among the constituents, M2 and K1 were found to be the most energetic in the region, with amplitudes of approximately 2.5 cm/s on the inner shelf. The M2 amplitude is lower than values previously reported on the shelf off Goa (~5 cm/s; Subeesh et al., 2013). In contrast, the K1 constituent is stronger on the inner shelf than at the shelf off Goa (~1.5 cm/s; Subeesh et al., 2013). Tides in both bands propagate predominantly across isobaths, similar to those on the shelf (Subeesh et al. 2013). However, in the surf zone, currents in the tidal band propagate primarily along isobaths.

The hourly climatology of inner-shelf residual currents and wind speed indicates that both intensify during nighttime. Likewise, the hourly climatology of wave height in the surf zone also intensifies at night. A previous study by Aboobacker et al. (2014), based on wave modeling and measurements during May 2005, reported that sea breeze is strong along the Goa coast within ~45 km and plays a major role in generating wind waves. However, our measurements indicate that strong land breezes significantly influence both barotropic currents and wave height. Regarding the diurnal cycle, Vethamony et al. (2011) reported that the sea breeze reaches its maximum between 15:00 and 18:00 hrs in the northwest direction, but our observations in January show that during this period, the sea

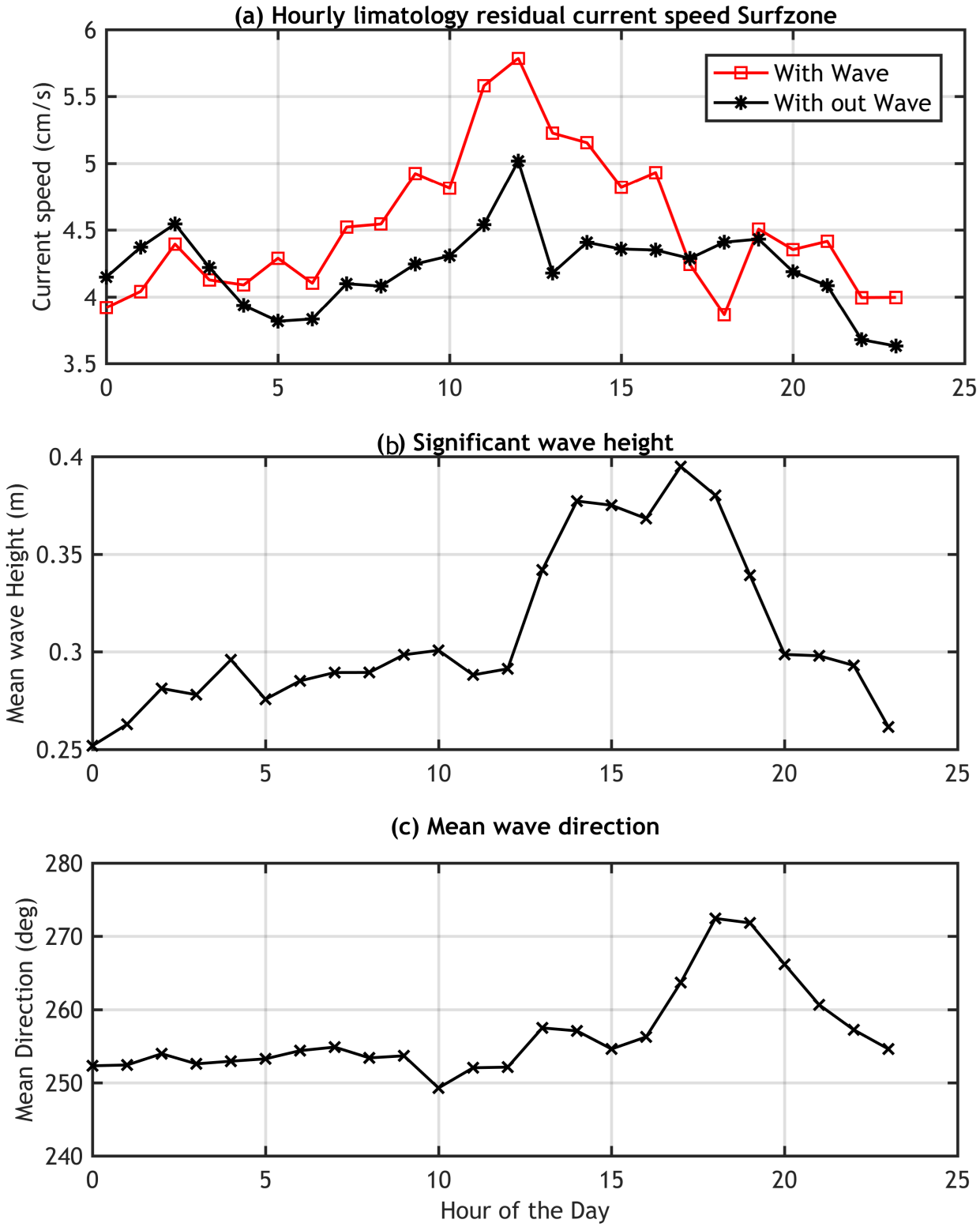

Figure 12. Hourly climatology of predicted surf-zone currents and associated forcing. The plots show the hourly climatology under two model configurations: with waves (red line) and without waves (black line) (a). Second panel shows the hourly climatology of the significant wave height (b) and the third mean wave direction (c).

breeze is predominantly directed towards the southeast.

The Delft3D hydrodynamic model, forced with tide, wave, and wind, is implemented for the inner shelf and surf zone to simulate barotropic currents in semidiurnal and diurnal bands. Various sensitivity analyses are performed to obtain optimum model settings to capture these currents. Sensitivity analysis of the Delft3D model extensively studied the effect of varying drag coefficients and roughness formulae and boundary conditions on prediction of tidal currents (Rahman and Venugopal, 2017; Pasma et al., 2024; Okon et al., 2025). Similarly, sensitivity analyses in this study revealed that small changes in bottom roughness, wind drag coefficients, and boundary conditions can significantly impact the performance of the model, especially when we considered spatially varying bottom roughness.

Including wave forcing improved model realism, showing the importance of wave-current coupled models to represent the shallow water dynamics in this region. Numerous research were discussed this interaction before: Allard et al. (2008), studied the Portuguese coast; Uchiyama et al. (2010), the California coast; Hopkins et al. (2016), southern shoreline of Martha's Vineyard; Song et al. (2020), southwestern Bohai Bay, China.

Sensitivity experiments with and without wind forcing showed the significant impact of winds on semidiurnal and diurnal currents in the surf zone. However, this effect is minimal in the inner shelf barotropic currents in these bands. Therefore, for accurate prediction of currents in the surf zone, it is essential to consider wind parameters in addition to wave and tidal forcing. Rafiq et al. (2020) also studied the effect of land-sea breeze on surface current in the southwest coast of Australia, where the surface currents near the coast show better correlation with wind.

This study also highlights the critical role of wave height and direction in driving currents within the surf zone. Observations indicate that daytime peaks in current speed are primarily associated with the prevailing wave approach angle and, to a lesser extent, wave height. However, as these findings are based on only five days' of field measurements, they cannot be considered conclusive. However, model simulation data from the surf zone indicates that wave height and direction have a significant influence on current speed, with stronger currents being produced by obliquely incident waves and increases in wave height during the day. Prakash et al. (2021) stated that nearshore currents in the north Goa region were influenced by prevailing wave and tide characteristics. And the influence of wave direction on longshore currents and sediment transport along the east coast of India was also reported by Balaji et al. (2019).

Overall, the study highlights the importance of including wind, and tide in addition to other forcing parameters when modeling the circulation in surf zone regions. It might be highly advantageous to use the Delft3D model to more precisely forecast how tidal currents will spread from the inner shelf to the coastal dynamics of the surf zone. As future work, a 3D baroclinic tidal model has to incorporate more consistent measurements from the surf zone to gain more understanding of cross-shore interactions and the dynamic exchange between the inner shelf and the surf zone. The complex interactions among tides, winds, and waves in shallow coastal regions necessitate detailed monitoring through comprehensive observations and high-resolution coastal modeling to ensure environmental sustainability.

Acknowledgements

The authors gratefully acknowledge the Directors of the Naval Physical and Oceanographic Laboratory-DRDO, Kochi, and the CSIR-National Institute of Oceanography, Goa. We also place our gratitude to the technical staff, scientists, and project staff for their assistance during the data collection program. We thank two reviewers for their suggestions to improve the manuscript. This is CSIR-NIO contribution number 7598.

Supplementary material

Supplementary material associated with this article can be found here.

Conflict of interest

None declared.

References

Aboobacker, V.M., Seemanth, M., Samiksha, S.V., Sudheesh, K., Kerkar, J., Vethamony, P., 2014. *Sea breeze-induced wind sea growth in the central west coast of India*. Ocean Eng. 84, 20–28. https://doi.org/10.1016/j.oceaneng.2014.03.030

Alford, M.H., Simmons, H.L., Marques, O.B., Girton, J.B., 2019. *Internal tide attenuation in the North Pacific*. Geophy. Res. Lett. 46 (14), 8205–8213. https://doi.org/10.1029/2019GL082648

Allard, R., Dykes, J., Hsu, Y.H.L., Kaihatu, J., Conley, D., 2008. *A real-time nearshore wave and current prediction system*. J. Marine Syst. 69 (1–2), 37–58. https://doi.org/10.1016/j.jmarsys.2007.02.020

Allouche, M., Bou-Zeid, E., Iipponen, J., 2023. *The influence of synoptic wind on land-sea breezes*. Q. J. Roy. Meteor. Soc. 149 (757), 3198–3219. https://doi.org/10.1002/qj.4552

Alvares, C., 1993. *Fish, Curry, and Rice: A Citizen's Report on the State of the Goan Environment*. Ecoforum, 1st edn., Goa, 260 pp.

Amol, P., Vijith, V., Fernando, V., Pednakar, P., Singh, J., 2018. *Impact of local and remote winds on the shelf circulation off the central west coast of India*. Ocean. Dynam. 68,

1607–1623.
https://doi.org/10.1007/s10236-018-1211-3

Andutta, F.P., Patterson, R.G., Wang, X.H., 2019. *Monsoon driven waves superpose the effect from macro-tidal currents on sediment resuspension and distribution*. Estuar. Coast. Shelf. Sci. 223, 85–93.
https://doi.org/10.1016/j.ecss.2019.04.036

Balaji, R., Ramana Murthy, M.V., Satheeshkumar, J., 2019. *Measurement of surf zone hydrodynamics along the coastline of Pondicherry, India*. [In:] *Proceedings of the Fourth International Conference in Ocean Engineering (ICOE2018)*, Vol. 2, Springer, Singapore, 25–34.
https://doi.org/10.1007/978-981-13-3134-3_3

Basco, D.R., 1983. *Surf zone currents*. Coast. Eng. 7 (4), 331–355.
https://doi.org/10.1016/0378-3839(83)90003-0

Chaudhuri, A., Amol, P., Shankar, D., Mukhopadhyay, S., Aparna, S.G., Fernando, V., Kankonkar, A., 2021. *Observed variability of the West India Coastal Current on the continental shelf from 2010–2017*. J. Earth. Syst. Sci. 130 (2), 77.
https://doi.org/10.1007/s12040-021-01603-4

Delpey, M., Lastiri, X., Abadie, S., Roeber, V., Maron, P., Liria, P., Mader, J., 2021. *Characterization of the wave resource variability in the French Basque coastal area based on a high-resolution hindcast*. Renew. Energ. 178, 79–95.
https://doi.org/10.1016/j.renene.2021.05.167

Dyer, K.R., 1997. *Estuaries: A Physical Introduction*. 2nd edn., Wiley, Chichester, 195 pp.

Galparsoro, I., Borja, Á., Legorburu, I., Hernández, C., Chust, G., Liria, P., Uriarte, A., 2010. *Morphological characteristics of the Basque continental shelf (Bay of Biscay, northern Spain); their implications for Integrated Coastal Zone Management*. Geomorphology 118 (3–4), 314–329.
https://doi.org/10.1016/j.geomorph.2010.01.012

George, J., Kumar, V.S., Gowthaman, R., Singh, J., 2020. *Nearshore waves and littoral drift along a micro-tidal wave-dominated coast having comparable wind-sea and swell energy*. J. Mar. Sci. Eng. 8 (1), 55.
https://doi.org/10.3390/jmse8010055

Halsne, T., Benetazzo, A., Barbariol, F., Christensen, K.H., Carrasco, A., Breivik, Ø., 2024. *Wave modulation in a strong tidal current and its impact on extreme waves*. J. Phys. Oceanogr. 54 (1), 131–151.
https://doi.org/10.1175/JPO-D-23-0051.1

Hamm, L., 1992. *Directional nearshore wave propagation over a rip channel: an experiment*. [In:] Edge, B.L. (Ed.), *Coastal Engineering 1992. Proceedings of the twenty-third international conferrence*, ASCE, New York, 226–239.
https://doi.org/10.1061/9780872629332.017

Holman, R.A., 1986. *Extreme value statistics for wave run-up on a natural beach*. Coast. Eng. 9 (6), 527–544.
https://doi.org/10.1016/0378-3839(86)90002-5

Hopkins, J., Elgar, S., Raubenheimer, B., 2016. *Observations and model simulations of wave-current interaction on the inner shelf*. J. Geophys. Res-Oceans, 121 (1), 198–208.
https://doi.org/10.1002/2015JC010788

Inman, D.L., Quinn, W.H., 1951. *Currents in the surf zone*. Coast. Eng. Proc. 2, 3–3.
https://icce-ojs-tamu.tdl.org/icce/article/view/1469

Jiao, N.Z., Chen, D.K., Luo, Y.M., Huang, X.P., Zhang, R., Zhang, H.B., Zhang, F., 2015. *Climate change and anthropogenic impacts on marine ecosystems and countermeasures in China*. Adv. Clim. Chang. Res. 6 (2), 118–125.
https://doi.org/10.1016/j.accre.2015.09.010

Kumar, N., Lerczak, J.A., Xu, T., Waterhouse, A.F., Thomson, J., Terrill, E.J., Ahn, S., 2021. *The inner-shelf dynamics experiment*. Bull. Amer. Meteor. Soc. 102 (5), E1033–E1063.
https://doi.org/10.1175/BAMS-D-19-0281.1

Kunte, P.D., Wagle, B.G., Sugimori, Y., 2002. *A review and re-assessment of sediment transport along the Goa Coast, India*. J. Coastal. Res. 18 (3), 612–621.
http://www.jstor.org/stable/4299114

Lentz, S.J., 1994. *Current dynamics over the northern California inner shelf*. J. Phys. Oceanogr. 24 (12), 2461–2478.
https://doi.org/10.1175/1520-0485(1994)024

Longuet-Higgins, M.S., 1970b. *Longshore currents generated by obliquely incident sea waves*. J. Geophys. Res. 75 (33), 6790–6801.
https://doi.org/10.1029/JC075i033p06790

Luijendijk, A.P., 2001. *Validation, calibration and evaluation of Delft3D-FLOW model with ferry measurements*. M.Sc. thesis, Tech. Univ. Delft, The Netherlands.

Matsunaga, N., Hashida, M., Kawakami, H., 1996. *Wind-induced waves and currents in a nearshore zone*. [In:] *Coastal Engineering 1996*, ASCE, New York, 3363–3377.
https://doi.org/10.1061/9780784402429.260

Mazumdar, A., 2020. *Recent contributions to the geochemistry and sedimentology of estuaries, mangroves, and mudbanks along the Indian coast: A status report*. Proc. Indian Natl Sci. Acad. 86 (1), 485–497.

Mehra, P., Prabhudesai, R.G., Joseph, A., Kumar, V., Agarvadekar, Y., Luis, R., Nadaf, L., 2013. *Comparison of sea-level measurements between microwave radar and subsurface pressure gauge deployed at select locations along the coast of India*. J. Appl. Remote. Sens. 7 (1), 073569–073569.
https://doi.org/10.1117/1.JRS.7.073569

Mitra, A., Mandal, S., Shanas, P.R., Joseph, D., Yuvaraj, S., George, J., Kumar, V.S., 2022. *Variability in tidal harmonics of the coastal and estuarine waters of Goa during the winter monsoon and spring inter-monsoon*. Reg. Stud. Mar. Sci. 51, 102226.
https://doi.org/10.1016/j.rsma.2022.102226

Moulton, M., Chickadel, C.C., Thomson, J., 2021. *Warm and cool nearshore plumes connecting the surf zone to the inner shelf*. Geophy. Res. Lett. 48 (10), e2020GL091675. https://doi.org/10.1029/2020GL091675

Müller, M., 2012. *The influence of changing stratification conditions on barotropic tidal transport and its implications for seasonal and secular changes of tides*. Cont. Shelf. Res. 47, 107–118. https://doi.org/10.1016/j.csr.2012.07.003

Okon, L.U.E., Seelam, J.K., Hemanath, L., Thomas, J., Narine, R., 2025. *Hypothesis-driven sensitivity analysis of Delft3D flexible mesh hydrodynamic model: insights into coastal processes in the monsoonal tropical Goa Coast, India*. Ocean Dynam. 75 (9), 1–14. https://doi.org/10.1007/s10236-025-01724-0

Paniagua-Arroyave, J.F., Valle-Levinson, A., Parra, S.M., Adams, P.N., 2019. *Tidal distortions related to extreme atmospheric forcing over the inner shelf*. J. Geophys. Res.-Oceans, 124(9), 6688—6701. https://doi.org/10.1029/2019JC015021

Pasma, G.R., Suharyanto, H.H.R., Khoirunnisa, H., Wijayanti, R., Gumbira, G., Rachman, R.A., 2024. *Assessment of sensitivity and validity of hydrodynamic model in Cisadane using Delft3D Flow model*. ILMU KELAUTAN: IJMS. 29 (1), 133–146. https://doi.org/10.14710/ik.ijms.29.1.133-146

Pitman, S., Gallop, S.L., Haigh, I.D., Masselink, G., Ranasinghe, R., 2016. *Wave breaking patterns control rip current flow regimes and surf zone retention*. Mar. Geol. 382, 176–190. https://doi.org/10.1016/j.margeo.2016.10.016

Port, A., Gurgel, K.W., Staneva, J., Schulz-Stellenfleth, J., Stanev, E.V., 2011. *Tidal and wind-driven surface currents in the German Bight: HFR observations versus model simulations*. Ocean. Dynam. 61 (10), 1567–1585. https://doi.org/10.1007/s10236-011-0412-9

Prakash, N., Ashly, K.U., Seelam, J.K., Bhaskaran, H., Yadhunath, E.M., Lavanya, H., Surisetty, V.A.K., 2021. *Investigation of near-shore processes along North Goa beaches: A study based on field observations and numerical modelling*. J. Earth. Syst. Sci. 130 (4), 242. https://doi.org/10.1007/s12040-021-01755-3

Pradhan, U.K., Mishra, P., Mohanty, P.K., Panda, U.S., Ramanamurthy, M.V., 2020. *Modeling of tidal circulation and sediment transport near tropical estuary, east coast of India*. Reg. Stud. Mar. Sci. 37, 101351. https://doi.org/10.1016/j.rsma.2020.101351

Pugh, D T., 1987. *Tides, surges and mean sea level*. 1st edn., John Wiley & Sons Ltd., United States, 486 pp.

Rafiq, S.W., Pattiaratchi, C., Janeković, I., 2020. *Dynamics of the land-sea breeze system and the surface current response in south-west Australia*. J. Mar. Sci. Eng. 8 (11), 931. https://doi.org/10.3390/jmse8110931

Rahman, A., Venugopal, V., 2017. *Parametric analysis of three-dimensional flow models applied to tidal energy sites in Scotland*. Estuar. Coast. Shelf. Sci. 189, 17–32. https://doi.org/10.1016/j.ecss.2017.02.027

Ren, L., Nash, S., Hartnett, M., 2015. *Observation and modeling of tide- and wind-induced surface currents in Galway Bay*. Water. Sci. Eng. 8 (4), 345–352. https://doi.org/10.1016/j.wse.2015.12.001

Rivonker, C.U., Padate, V.P., Hegde, M.R., Velip, D.T., 2018. *Habitat complexity of tropical coastal ecosystems: An ecosystem management perspective*. [In:] *Environmental Management of Marine Ecosystems*. CRC Press, 263–286.

Seelam, J.K., Yadhunath, E.M., Jishad, M., Gowthaman, R., Rajasekaran, C., Pednekar, P. S. 2014. *Post-monsoon equilibrium beach profiles and longshore sediment transport rates at Candolim, Miramar and Keri beaches of Goa*. Current Sci. India, 106 (3), 408–416. https://www.jstor.org/stable/24099901

Sharples, J., 1997. *Cross-shelf intrusion of subtropical water into the coastal zone of northeast New Zealand*. Cont. Shelf. Res. 17 (7), 835–857. https://doi.org/10.1016/S0278-4343(96)00060-X

Shenoi, S.S.C., Gouveia, A.D., Shetye, S.R., 1992. *Diurnal and semidiurnal tidal currents in the deep mid-Arabian Sea*. Proc. Indian Acad. Sci.-Earth Planet. Sci. 101, 177–189. https://doi.org/10.1007/BF02840351

Shetye, S.R., I. Suresh, I., Shankar, D., Sundar, S., Jayakumar, P., Mehra, R.G., Prabhudesai, R.G., Pednekar, P.S., 2008. *Observational evidence for remote forcing of the West India Coastal Current*. J. Geophys. Res.-Oceans. 113 (C11). https://doi.org/10.1029/2008JC004874

Sous, D., Forsberg, P.L., Touboul, J., Nogueira, G.G., 2021. *Laboratory experiments of surf zone dynamics under on- and offshore wind conditions*. Coast. Eng. 163, 103797. https://doi.org/10.1016/j.coastaleng.2020.103797

Song, H., Kuang, C., Wang, X.H., Ma, Z., 2020. *Wave-current interactions during extreme weather conditions in southwest of Bohai Bay China*. Ocean. Eng. 216, 108068. https://doi.org/10.1016/j.oceaneng.2020.108068

Stelling, G.S., Van Kester, J.A.T.M., 1994. *On the approximation of horizontal gradients in sigma coordinates for bathymetry with steep bottom slopes*. Int. J. Numer. Meth. Fl. 18 (10), 915–935. https://doi.org/10.1002/fld.1650181003

Sterl, M.F., Delandmeter, P., van Sebille, E., 2020. *Influence of barotropic tidal currents on transport and accumulation of floating microplastics in the global open ocean*. J. Geophys. Res-Oceans, 125 (2), e2019JC015583. https://doi.org/10.1029/2019JC015583

Stow, D., 2017. *Oceans: A Very Short Introduction*. Oxford Univ. Press, 224 pp. https://doi.org/10.1093/actrade/9780199655076.

001.0001

Subeesh, M.P., Unnikrishnan, A.S., 2016. *Observed internal tides and near-inertial waves on the continental shelf and slope off Jaigarh, central west coast of India*. J. Marine Syst. 157, 1–19. https://doi.org/10.1016/j.jmarsys.2015.12.005

Subeesh, M.P., Unnikrishnan, A.S., Fernando, V., Agarwadekar, Y., Khalap, S.T., Satelkar, N.P., Shenoi, S.S.C., 2013. *Observed tidal currents on the continental shelf off the west coast of India*. Cont. Shelf. Res. 69, 123–140. https://doi.org/10.1016/j.csr.2013.09.008

Subeesh, M.P., Unnikrishnan, A.S., Francis, P.A., 2021. *Generation, propagation and dissipation of internal tides on the continental shelf and slope off the west coast of India*. Cont. Shelf. Res. 214, 104321. https://doi.org/10.1016/j.csr.2020.104321

Testut, L., Unnikrishnan, A.S., 2016. *Improving modeling of tides on the continental shelf off the west coast of India*. J. Coastal. Res. 32 (1), 105–115. http://drs.nio.org/drs/handle/2264/4908

Truong, D.T., Doan, D., Nguyen Cao, D., 2021. *The impact of waves and tidal currents on the sediment transport at the sea port*. Civil. Eng. J. 7 (10), 1634–1649. https://doi.org/10.28991/cej-2021-03091749

Uchiyama, Y., McWilliams, J.C., Shchepetkin, A.F., 2010. *Wave–current interaction in an oceanic circulation model with a vortex-force formalism: Application to the surf zone*. Ocean. Model. 34 (1–2), 16–35. https://doi.org/10.1016/j.ocemod.2010.04.002

Venkateswarlu, C., Surisetty, V.A.K., Somani, A., Gireesh, B., Naidu, C.V., 2023. *Surf zone-related drownings and injuries based on lifeguard records in Goa beaches (2008–2020)*. Nat. Hazards 117 (1), 313–337. https://doi.org/10.1007/s11069-023-05861-x

Vethamony, P., Aboobacker, V.M., Menon, H.B., Kumar, K.A., Cavaleri, L., 2011. *Superimposition of wind seas on pre-existing swells off Goa coast*. J. Marine Syst. 87 (1), 47–54. https://doi.org/10.1016/j.jmarsys.2011.02.024

Wright, L.D., Short, A.D., 1984. *Morphodynamic variability of surf zones and beaches: a synthesis*. Mar. Geol. 56 (1–4), 93–118. https://doi.org/10.1016/0025-3227(84)90008-2

Yadhunath, E.M., Seelam, J.K., Jishad, M., 2022a. *Rip current occurrences in meso tidal surf zones at a coastal stretch along the central west coast of India*. Reg. Stud. Mar. Sci. 51, 102180. https://doi.org/10.1016/j.rsma.2022.102180

Yadhunath, E.M., Seelam, J.K., Pednekar, P.S., Rajive, R.K., Gowthaman, R., 2022b. *Longshore currents on a meso-tidal beach of Goa, India – Measurements and improved formulae*. Indian. J. Geo.-Mar. Sci. 51 (11), 867–877. https://doi.org/10.56042/ijms.v51i11.3503